


Lecture 10. Surface Energy Balance (Garratt 5.1-5.2)

The balance of energy at the earth's surface is inextricably linked to the overlying atmospheric boundary layer. In this lecture, we consider the energy budget of different kinds of surfaces. Consider first an ideal surface, which is a very thin interface between the air and an underlying solid or liquid medium that is opaque to radiation. Because it is thin, this surface has negligible heat capacity, and conservation of energy at the surface requires that

$$R_N = H_S + H_L + H_G.$$


where (note sign conventions)

H_S (often just called H) is the upward surface sensible heat flux

$H_L = LE$ is the upward surface latent heat flux due to evaporation at rate E

H_G is the downward ground heat flux into the subsurface medium.

R_N is the net downward radiative flux (longwave + shortwave).

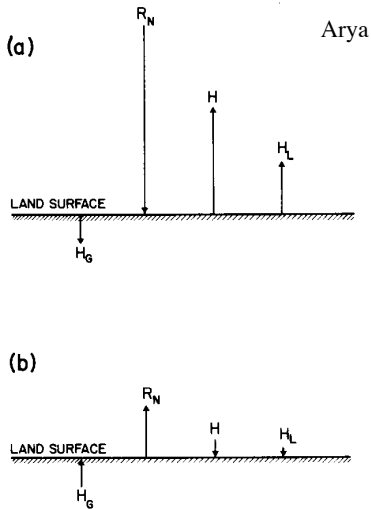


Fig. 2.1 Schematic representation of typical surface energy budgets during (a) daytime and (b) nighttime.

The ratio $B = H_L/H_S$ is called the **Bowen ratio**. $L = 2.5 \times 10^6 \text{ J kg}^{-1}$ is the latent heat of vaporization. Over land, there is a large diurnal variation in the surface energy budget (see schematic below). Over large bodies of water, the large heat capacity of the medium and the absorption of solar radiation over a large depth combine to reduce the near-surface diurnal temperature variability, so H_S and H_L vary much less. However, the surface ‘skin temperature’ of a tropical ocean can vary diurnally by up to 3 K in sunny, light-wind conditions.

An ideal surface is not usually encountered. Real surfaces may include a plant canopy or other features such as buildings not opaque to radiation and with a significant heat capacity. In this case, it is more appropriate to define an interfacial layer which includes such features. We let $W(t)$ be the energy stored within this layer per unit horizontal area. The revised layer energy budget is:

$$R_N = H_S + H_L + H_G + dW/dt.$$



We could also consider the energy budget of control volumes with finite horizontal extent (e.g. a parking lot, city, or larger geographic region). In this case horizontal transfer of energy may also be important; we won't consider this complication here.

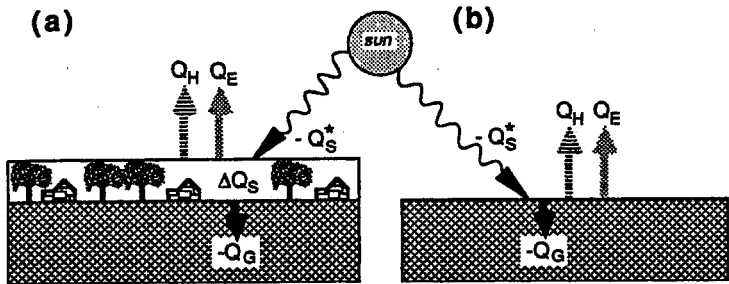


Fig. 7.2 Contributions to the surface energy balance (a) for a finite thickness box and (b) for an infinitesimally thin layer. $-Q_S^*$ is the net radiative contribution, Q_H is turbulent sensible heat flux, Q_E is turbulent latent heat flux, $-Q_G$ is molecular flux into the ground, and ΔQ_S is storage.

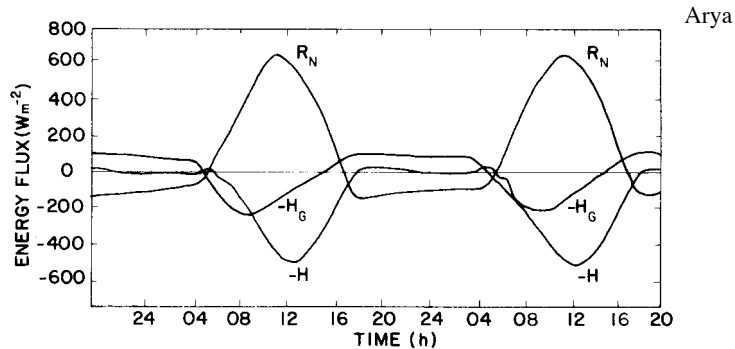
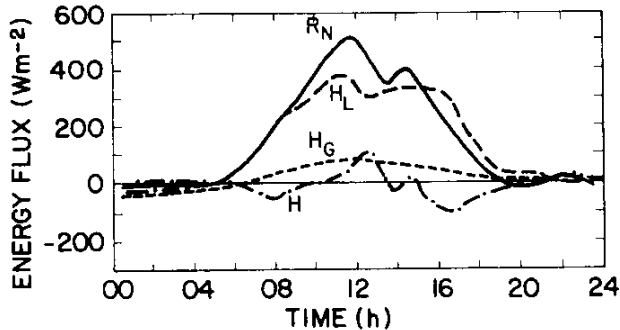


Fig. 2.3 Observed diurnal energy balance over a dry lake bed at El Mirage, California, on June 10 and 11, 1950. [After Vehrencamp (1953).]

Examples

The energy budget measured over a dry desert lake bed is shown above. In this case, latent heat fluxes are negligible. During the day, copious solar radiation is absorbed at the surface, and the ground heats up rapidly. Initially, most of the heat is conducted down into the soil, but as the layer of warmed soil thickens, H_G dominates; the heat is primarily transferred to the air. This is promoted by extreme differences (up to 28 K) between the ground temperature and the 2 m air temperature. At night, surface radiative cooling is balanced by an upward ground heat flux. Since the nocturnal boundary layer is very stable, the turbulent heat flux H_G is negligible.

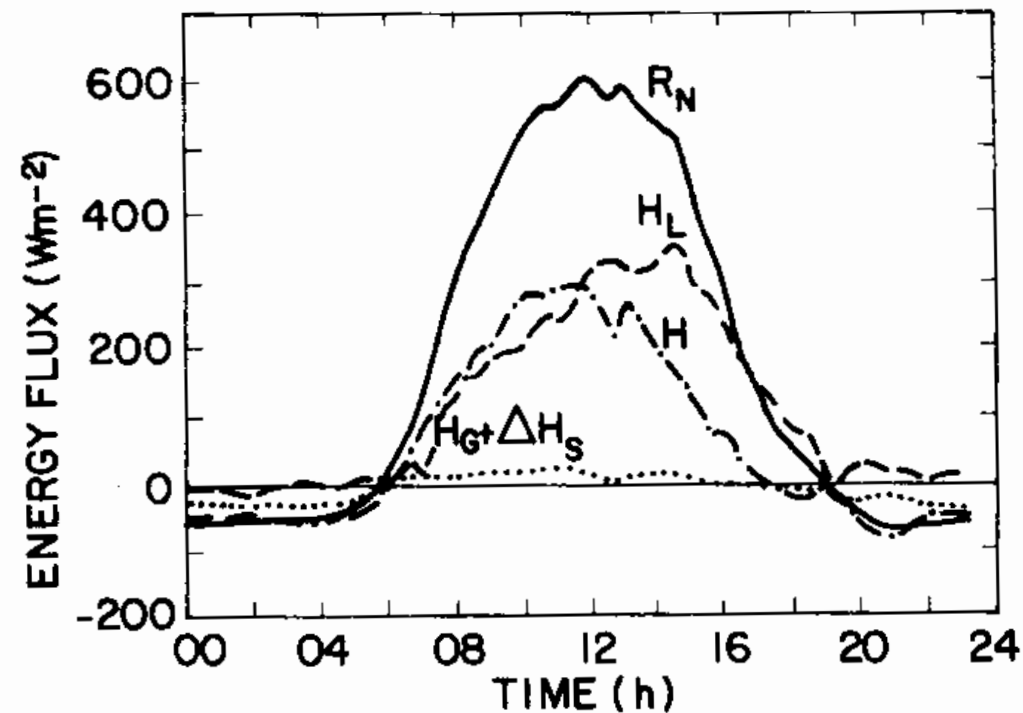
The energy budget of a barley field is shown below. During the daytime, radiative heating of the surface is balanced mainly by latent heat flux due to **evapotranspiration**, i. e. evaporation from the soil surface and transpiration by the plant leaves. In the lingo, the Bowen ratio is small, -0.3 to 0.3. H_L can be so large that the surface gets cooler than the air during early morning and late afternoon and the heat flux is downward. For a field, heat storage is usually negligible. At night, all terms become much smaller; as before, radiative cooling is mainly balanced by ground heat flux..



Arya

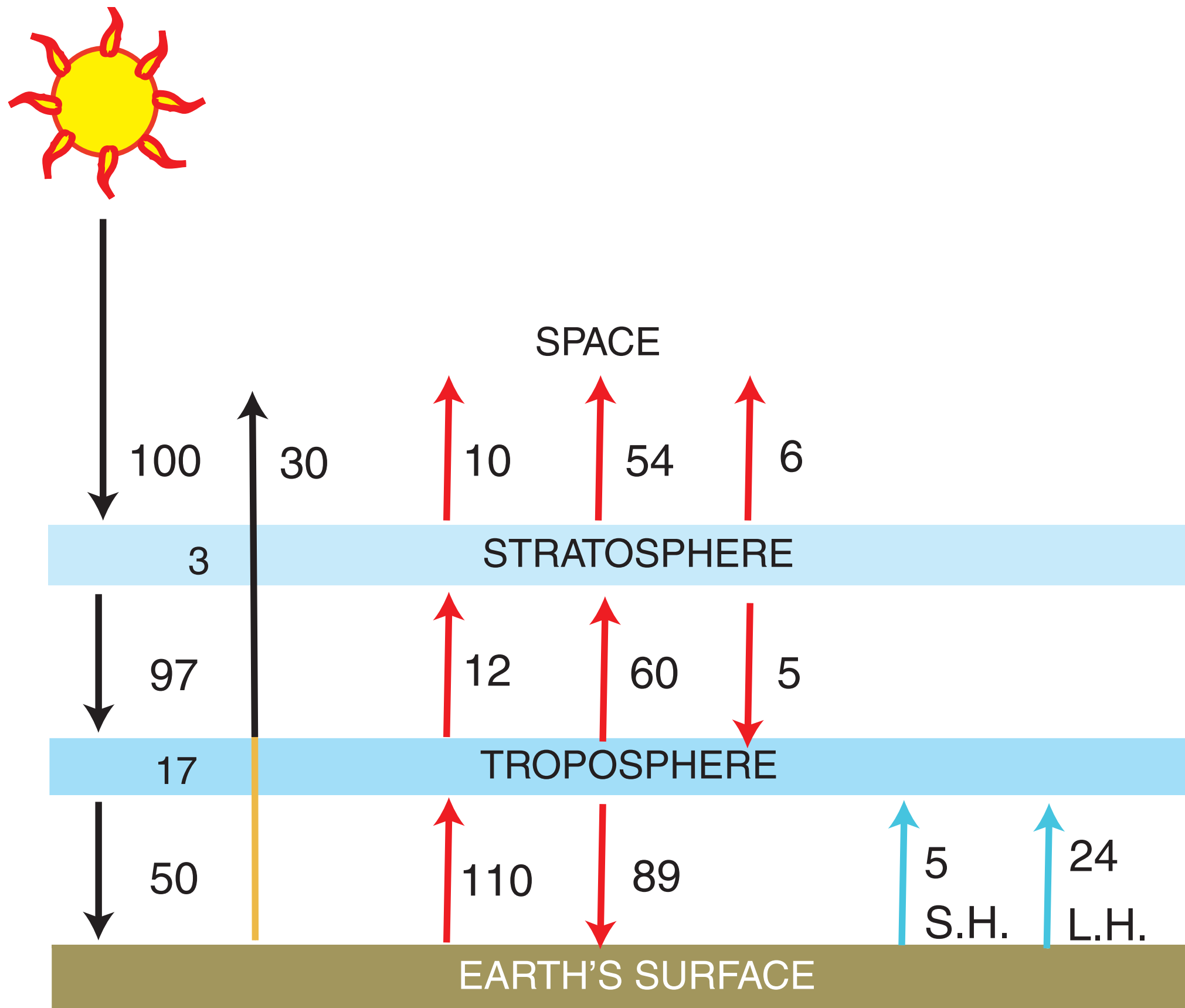
Fig. 2.4 Observed diurnal energy budget of a barley field at Rothamsted, England, on July 23, 1963. [From Oke (1987); after Long *et al.* (1964).]

The last example is a Douglas fir forest (next page). Here latent and sensible heat fluxes are comparable during the day. The storage and ground heat flux are lumped in the curves, but for deep forest, the storage term dominates. At night, release of heat from the tree canopy and condensation (dew) balance radiative energy loss.



Arya

Fig. 2.5 Observed energy budget of a Douglas fir canopy at Haney, British Columbia, on July 23, 1970. [From Oke (1987); after McNaughton and Black (1973).]



Adapted from Dennis L. Hartmann, *Global Physical Climatology*, p. 28
(Copyright 1994), with permission from Elsevier.

Net radiation at the surface

The net radiation R_N is due to the difference between downwelling and upwelling shortwave plus longwave radiative fluxes. The net shortwave flux depends on the incident solar radiation $R_{s\downarrow}$ and on surface albedo a_s . The net longwave flux depends upon the downwelling longwave radiation $R_{L\downarrow}$, the surface emissivity ϵ_s , and the radiating temperature T_s :

$$R_N = R_{s\downarrow} - R_{s\uparrow} + R_{L\downarrow} - R_{L\uparrow} = (1 - a_s)R_{s\downarrow} + R_{L\downarrow} - \{(1 - \epsilon_s)R_{L\downarrow} + \epsilon_s \sigma T_s^4\}$$

Thus, the surface characteristics critically influence R_N . A table of typical surface radiative characteristics is given below. Albedos are quite diverse, while emissivities are usually near, but not equal, to 1.

Table 3.1
Radiative Properties of Natural Surfaces^a

Surface type	Other specifications	Albedo (<i>a</i>)	Emissivity (ϵ)
Water	Small zenith angle	0.03–0.10	0.92–0.97
	Large zenith angle	0.10–0.50	0.92–0.97
Snow	Old	0.40–0.70	0.82–0.89
	Fresh	0.45–0.95	0.90–0.99
Ice	Sea	0.30–0.40	0.92–0.97
	Glacier	0.20–0.40	
Bare sand	Dry	0.35–0.45	0.84–0.90
	Wet	0.20–0.30	0.91–0.95
Bare soil	Dry clay	0.20–0.35	0.95
	Moist clay	0.10–0.20	0.97
	Wet fallow field	0.05–0.07	
Paved	Concrete	0.17–0.27	0.71–0.88
	Black gravel road	0.05–0.10	0.88–0.95
Grass	Long (1 m)	0.16–0.26	0.90–0.95
	Short (0.02 m)		
Agricultural	Wheat, rice, etc.	0.10–0.25	0.90–0.99
	Orchards	0.15–0.20	0.90–0.95
Forests	Deciduous	0.10–0.20	0.97–0.98
	Coniferous	0.05–0.15	0.97–0.99

^a Compiled from Sellers (1965), Kondratyev (1969), and Oke (1978).

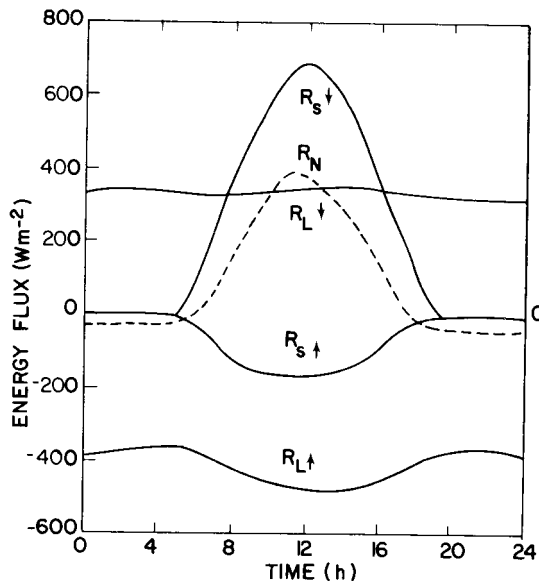
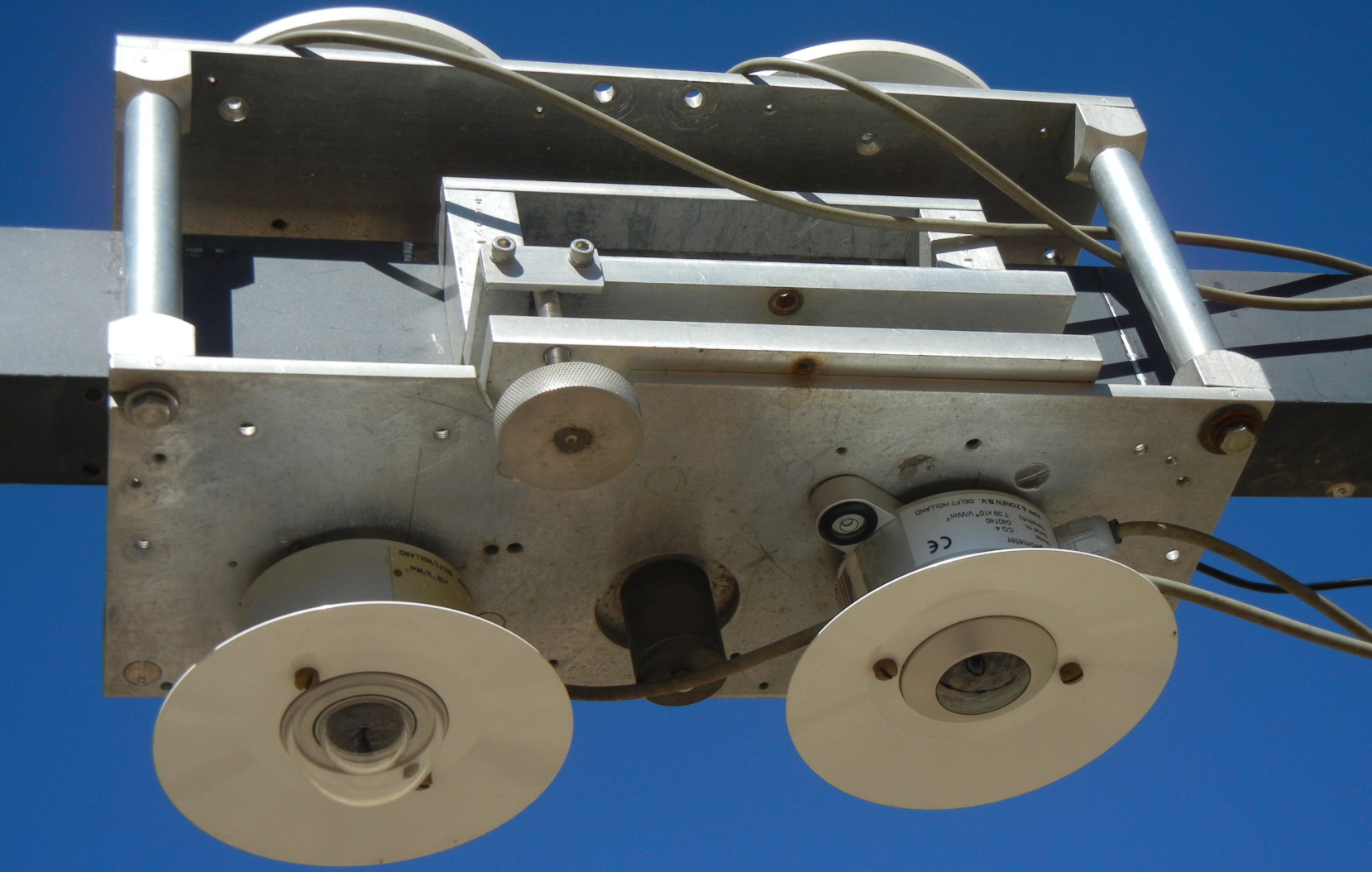


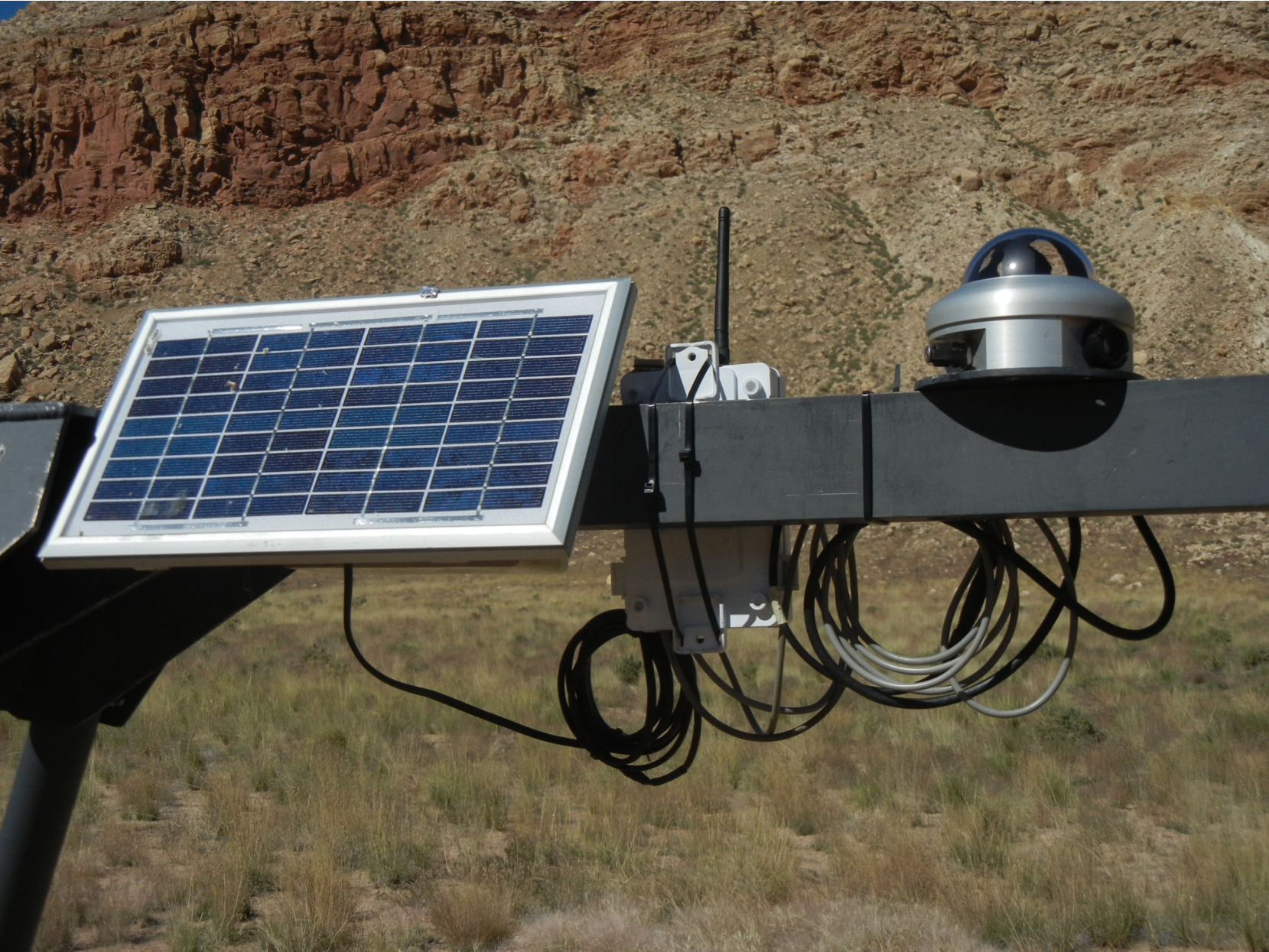
Fig. 3.4 Observed radiation budget over a 0.2-m-tall stand of native grass at Matador Saskatchewan, on July 30, 1971. [From Oke (1987); after Ripley and Redmann (1976).]

An example of the surface radiation components is shown above.









Soil temperatures and heat flux

The surface or skin temperature is important for the radiative balance of the surface and for predicting frost and dew. It can be quite different than the 'surface' air temperature, which is conventionally measured at 1.5-2 m. In fact, it can be difficult to even measure *in situ* because it is difficult to shield and ventilate a sensor placed at the surface. Furthermore, if there is a plant canopy or surface inhomogeneity, there is no single uniquely definable surface temperature. Radiatively, an apparent surface temperature can be determined from the upward longwave energy flux if the emissivity is known. Large diurnal variations in skin temperature are achieved for bare, dry surfaces in clear calm conditions. Under such conditions, midday skin temperature may reach 50-60 C, while early morning skin temperatures can drop to 10-20 C.

The surface temperature is related to the profile of temperature in the subsurface medium, as illustrated in the figures on the next page. In a solid medium, the subsurface temperature profile is governed by heat conduction. Deeper in the soil, the diurnal temperature cycle decreases and lags the cycle of skin temperature. Over an annual cycle, similar waves penetrate further into the soil.

Observed annual subsurface soil temperature variability (Arya)

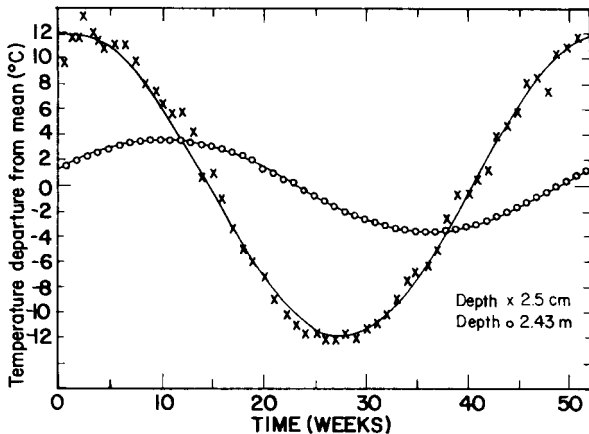
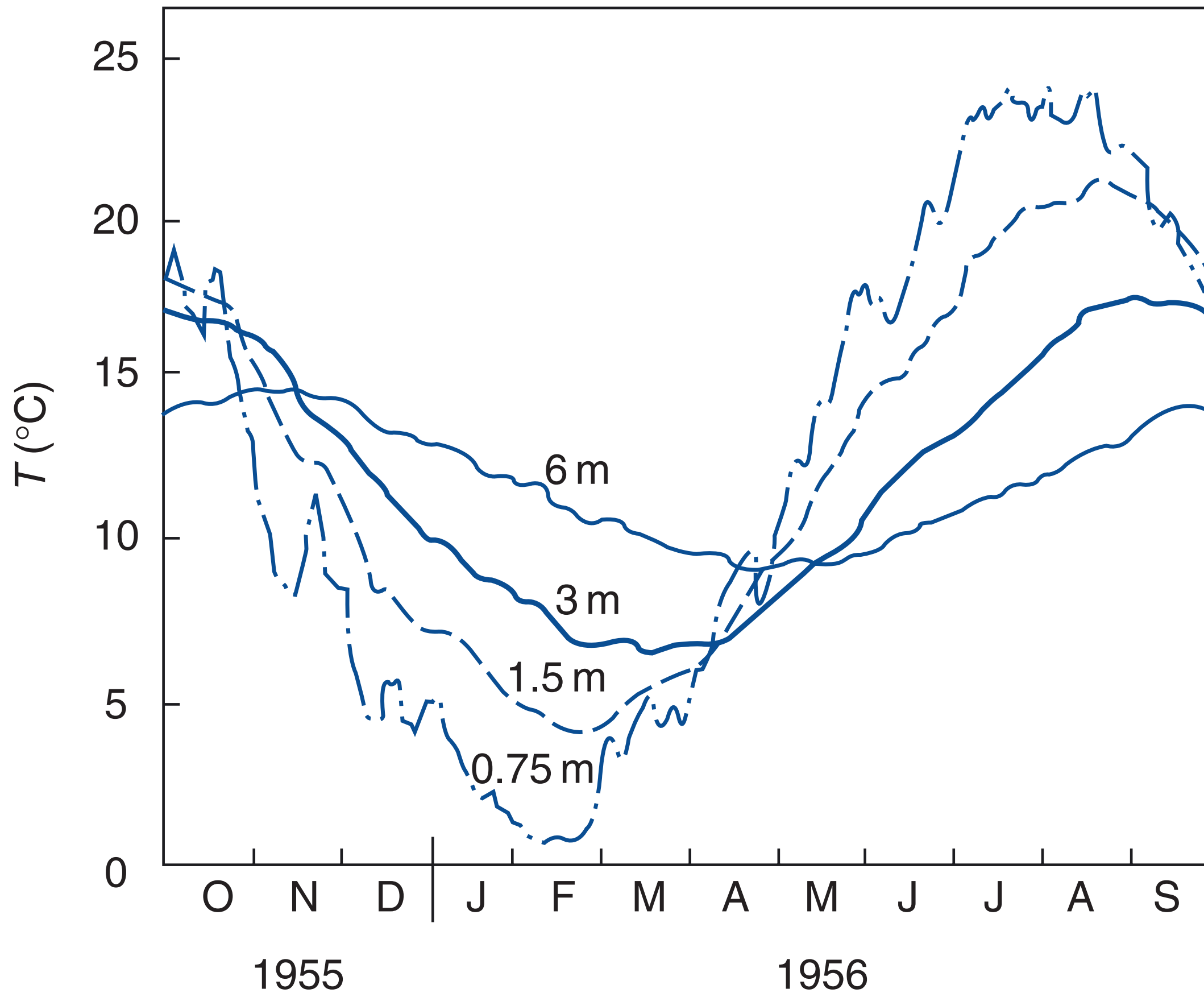


Fig. 4.2 Annual temperature waves in the weekly averaged subsurface soil temperatures at two depths in a sandy loam soil. ×, 2.5 cm; ○, 2.43 m. Fitted solid curves are sine waves. [From Deacon (1969); after West (1952).]

Soil temperature at 4 levels below the surface



Observed diurnal subsurface soil temperature variability (Arya)

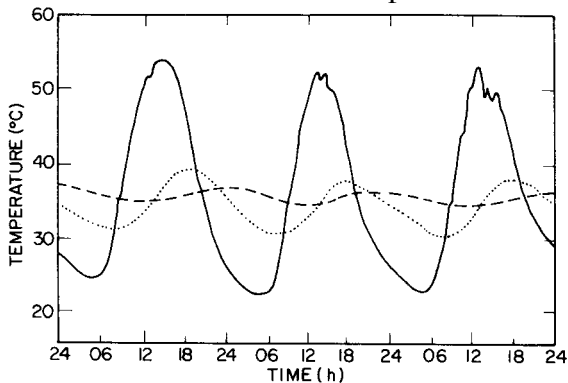
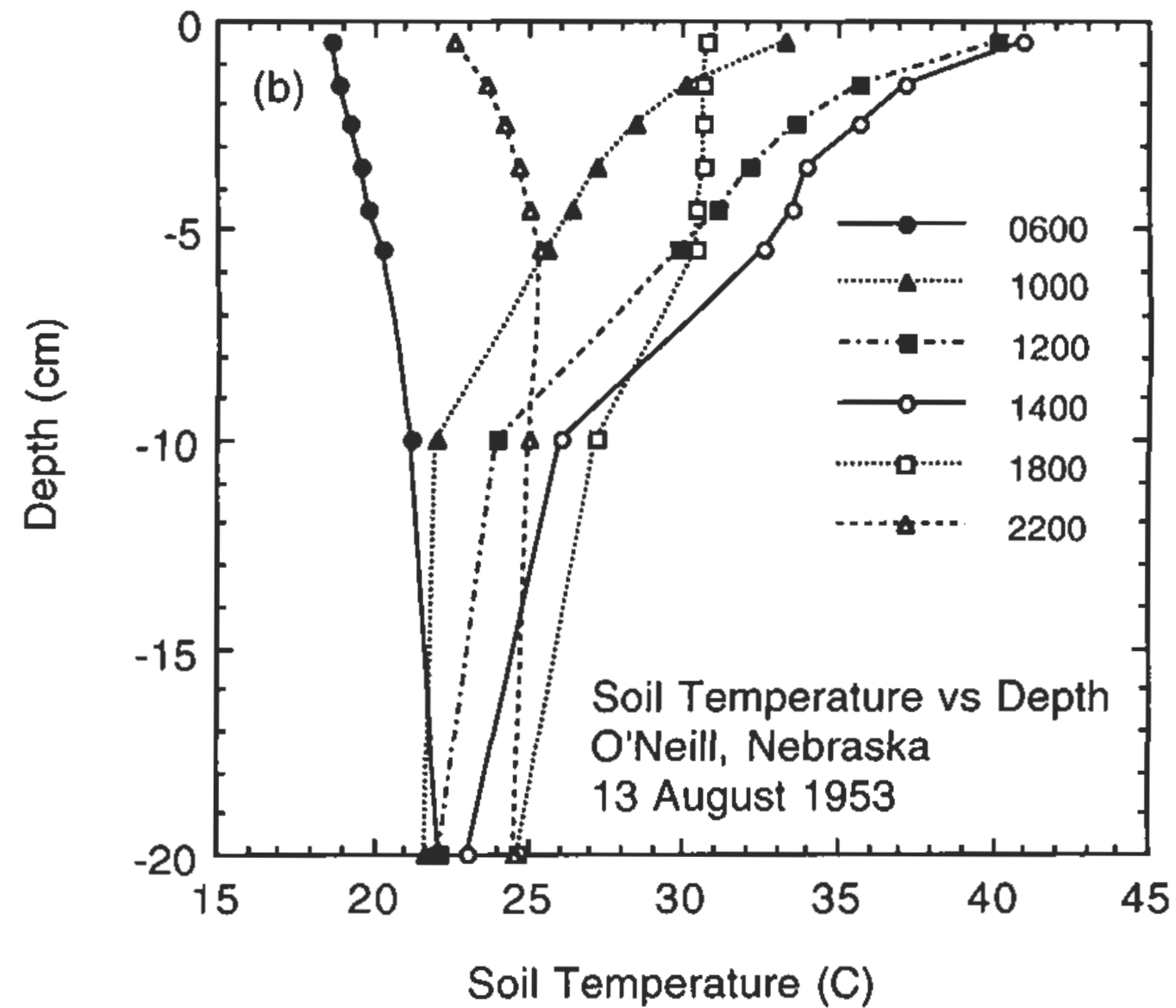
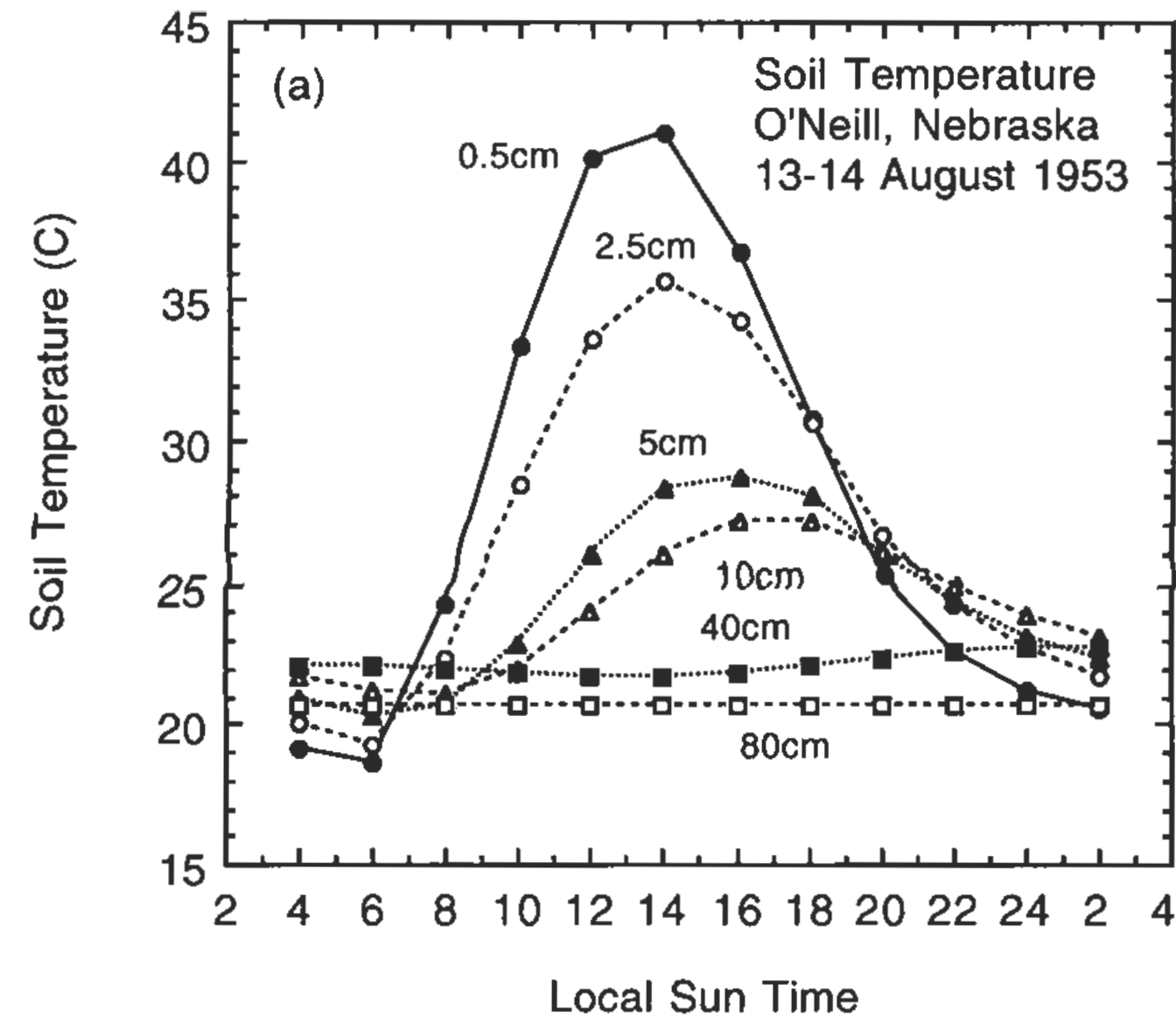


Fig. 4.1 Observed diurnal course of subsurface soil temperatures at various depths in a sandy loam with bare surface. —, 2.5 cm; ····, 15 cm; ---, 30 cm. [From Deacon (1969); after West (1952).]

Soil temperature at various depths under a grass field



If z is depth into the soil and $T(z, t)$ is soil temperature, Fourier's law of heat conduction states:

$$H_G = -k \partial T / \partial z, \quad (k = \text{thermal conductivity})$$

Thermal energy conservation implies that

$$\rho c \frac{\partial T}{\partial t} = - \frac{\partial H_G}{\partial z} \quad (\rho = \text{density}, c = \text{heat capacity})$$

Combining these two equations and assuming that the subsurface medium is homogeneous, so that material constants do not depend on z , we obtain the diffusion equation

$$\frac{\partial T}{\partial t} = \kappa \frac{\partial^2 T}{\partial z^2} \quad (\kappa = k/\rho c = \text{thermal diffusivity}) \quad (1)$$

A table of material properties is given below; the thermal conductivity varies over almost two orders of magnitude from new snow (low) to rock (high). Wet soils have conductivities about five times as large as dry soils. The thermal diffusivity shows similar trends, but less variation. Surprisingly, κ is smallest for water due to its large heat capacity.

Table A7. *Representative values of the thermal conductivity k_s , specific heat c_s , density ρ_s and thermal diffusivity κ_s for various types of surface based mainly on Table 11-3 in Pielke (1984)*

Garratt

Data for clay and sand are approximately consistent with Eq. A24, in which C_{si} is equal to 2.7×10^6 and $2.2 \times 10^6 \text{ J m}^{-3} \text{ K}^{-1}$ for clay and sand respectively; C_w is equal to $\rho_w c_1$, with $\rho_w = 1000 \text{ kg m}^{-3}$ and $c_1 = 4186 \text{ J kg}^{-1} \text{ K}^{-1}$; and η_s is taken from Table A9. The reader should also consult e.g. Geiger (1965, Table 10), Hillel (1982, Table 9.3) and Oke (1987, Table 2.1).

Surface	k_s ($\text{W m}^{-1} \text{ K}^{-1}$)	c_s ($\text{J kg}^{-1} \text{ K}^{-1}$)	ρ_s (kg m^{-3})	κ_s ($10^{-6} \text{ m}^2 \text{ s}^{-1}$)
<i>Sand soil</i>				
dry	0.3	800	1600	0.23
$\eta = 0.2$	1.9	1260	1800	0.84
$\eta = 0.4$	2.2	1480	2000	0.74
<i>Clay soil</i>				
dry	0.25	890	1600	0.18
$\eta = 0.2$	1.1	1170	1800	0.52
$\eta = 0.4$	1.6	1550	2000	0.52
<i>rock</i>	2.9	750	2700	1.4
<i>ice</i>	2.5	2100	910	1.3
<i>snow</i>				
old	1.0	2090	640	0.7
new	0.1	2090	150	0.3
<i>water</i>	0.6	4186	1000	0.14

In the case of sinusoidal forcing, we take the upper boundary condition (at $z=0$) to be

$$T(0, t) = \bar{T} + A \cos \omega t,$$

where $T(0, t)$ is the surface temperature, A is the surface temperature amplitude, \bar{T} is the average surface temperature and ω is the angular frequency. For the lower boundary condition, we assume that the deep soil temperature is equal to the average surface temperature: $T(\infty, t) = \bar{T}$. A general solution to (3) is

$$T(z, t) = \bar{T} + \text{Re}\{a(z) \exp(i\omega t)\}, \quad (4)$$

where $a(z)$ is a complex amplitude. Substitute (4) into (3) to get

$$i\omega a = -\kappa \frac{d^2 a}{dz^2}. \quad (5)$$

To satisfy the boundary conditions on T , we require $a(0) = A$ and $a(z \rightarrow \infty) = 0$.

The solution of (5) that satisfies the boundary conditions on a is

$$a(z) = A \exp \left(-[1 + i] \frac{z}{D} \right), \quad (6)$$

where D is referred to as the *damping depth* and is given by

$$D = (2\kappa/\omega)^{1/2}. \quad (7)$$

Now use (6) in (4), $e^a e^b = e^{a+b}$, and $\exp(ix) = \cos(x) + i \sin(x)$ to obtain

$$T(z, t) = \overline{T} + A \exp(-z/D) \cos(\omega t - z/D). \quad (8)$$

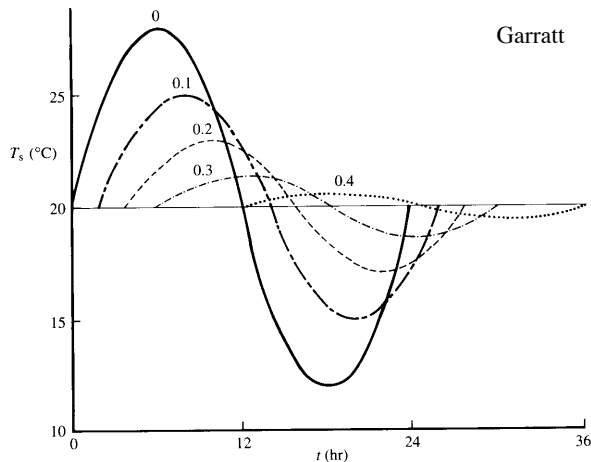


Fig. 5.1 Idealized variation of soil temperature through a diurnal cycle for several depths in the soil (indicated in metres). The curves represent the solutions to Eq. 5.7 for sinusoidal forcing; these are given by Eq. 5.8. A uniform soil is assumed with $\kappa_s = 0.8 \times 10^{-6} \text{ m}^2 \text{ s}^{-1}$ and $k_s = 1.68 \text{ W m}^{-1} \text{ K}^{-1}$.

$$T(z, t) = \bar{T} + \exp(-z/D) \cos(\omega t - z/D)$$

(3)

This solution is shown above. The temperature wave damps exponentially with depth z , and lags the surface temperature wave by a phase z/D , which increases with depth (see observations at bottom of page). The **damping depth D** to which the temperature wave penetrates increases as the oscillation frequency slows and is larger if the thermal diffusivity is larger. For moist soil ($\kappa = 0.8 \times 10^{-6} \text{ m}^2 \text{ s}^{-1}$), $D = 0.14 \text{ m}$ for the diurnal cycle and 2.8 m for the annual cycle.

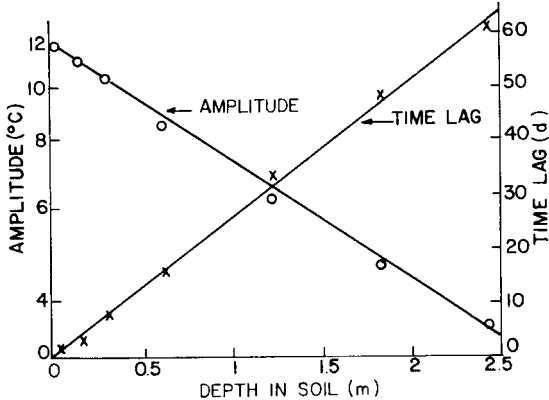


Fig. 4.4 Variations of amplitude and time lag of the annual soil temperature waves with depth in the soil. [From Deacon (1969).]

The ground heat flux at the surface is

$$H_G = -k \partial T / \partial z(0) = -kA/D \operatorname{Re}\{[1 + i] \exp(i\omega t)\} = \rho c(\kappa\omega)^{1/2} \cos(\omega t + \pi/4)$$

It leads the surface temperature wave by 1/8 cycle. Hence, the ground heat flux is largest three hours ahead of the surface temperature for a diurnally varying surface temperature cycle.

In practice, the diurnal cycle of surface temperature is not sinusoidal. Furthermore, the surface temperature interacts with the sensible and latent heat fluxes so that the surface boundary condition is really the energy balance of the surface, which is coupled to the atmosphere. Lastly, testing of these formulas is complicated by the fact the temperature within 1 cm of the ground can be non-uniform, so the surface temperature and ground heat flux must be inferred from measurements across a buried 'flux plate', a thin plate buried within the soil that measures heat flux based on the temperature difference across it, typically at a depth of 1-2 cm.

